

# Modeling of Chloride Transport in Cracked Concrete: A 3-D Image-based Microstructure Simulation

Yang Lu<sup>\*1</sup>, Edward Garboczi<sup>2</sup>, Dale Bentz<sup>3</sup>, Jeffrey Davis<sup>4</sup>

<sup>1,2,3,4</sup> National Institute of Standards and Technology

\*Corresponding author: Engineering Laboratory, National Institute of Standards and Technology, 100 Bureau Drive 8615, Gaithersburg, MD 20899, [yang.lu@nist.gov](mailto:yang.lu@nist.gov)

**Abstract:** It is highly desirable to develop a model predicting the chloride diffusion profile in cracked concrete while considering the real microstructure including cement paste, voids, and aggregates. While current models consider concrete at various levels of complexity in predicting the initiation of chloride-induced corrosion, considering the influence of cracking is generally beyond their scope. In this study, a 3-D image-based microstructure simulation procedure was developed to model the chloride ingress in cracked mortar. A micro-X-ray fluorescence (XRF) test was conducted to measure the chloride concentration profile of a mortar sample. The notched mortar sample was exposed in a chloride ponding test for 30 days before the micro-XRF measurement. A 2-D simulation result, with a mesh based directly on the XRF characterization of microstructure, showed good agreement with the micro-XRF measurement. With this validation, two different 3-D concrete microstructures were generated and meshed in 3-D and a commercial software package was used to accurately compute the influence of cracking on chloride diffusion with binding. The chloride concentration gradient in the crack changed the concentration profile along the crack and nearby irregular aggregate surfaces continually. Comparison to micro-XRF measurement data indicates that the contributions of the crack play a significant role in the chloride ingress.

**Keywords:** COMSOL Multiphysics, chloride diffusion and reaction, micro-X-ray fluorescence, X-ray CT, virtual concrete model, corrosion.

## 1. Introduction

To improve the service life of concrete structures and make them more durable, appropriate mechanical and transport properties are equally necessary. Generally, common concrete degradation processes, including

corrosion of steel reinforcement, sulfate attack, alkali-silica reaction, and damage due to freezing/thawing are strongly influenced by the diffusion of ions modified by any binding/reaction. Thus, an applicable approach to increase concrete service life is to reduce transport phenomena in concrete. Moreover, micro- or macro- cracks, which have a critical negative influence on all concrete degradation processes, are almost always present in concrete during its service life. Cracks with different widths and depths will reduce the effective cover thickness and accelerate the migration of chloride ions. Understanding the relationships between cracked microstructure and transport can improve the elucidation of degradation mechanisms within concrete. While current models consider concrete at various levels of complexity in predicting the initiation of chloride-induced corrosion, considering the influence of cracking is generally beyond their scope. This paper develops a model to predict the chloride diffusion depth in cracked concrete considering the real microstructure including cement paste, voids, and aggregates.

Previous research has used the COMSOL Multiphysics package<sup>1</sup> to model the microscale corrosion and cracking process in reinforced concrete due to non-uniform corrosion (Pan and Lu 2012). The properties of cracked and porous media were analyzed by COMSOL (Perko et al.). Reaction and diffusion processes in a mineral rock, without considering microstructure explicitly, were also studied by (Richter et al.). Some studies, based on non-steady state migration tests, were described in NT BUILD 492, using an electrical field and artificial cracks (Marsavina et al. 2009). (Kwon et al. 2009)

---

<sup>1</sup> Certain commercial equipment and/or materials are identified in this report in order to adequately specify the experimental procedure. In no case does such identification imply recommendation or endorsement by the National Institute of Standards and Technology, nor does it imply that the equipment and/or materials used are necessarily the best available for the purpose.

obtained the relationship between diffusion coefficients and crack widths in cracked concrete structures through field investigations; however, the crack depth is equally important and should be considered in the model. Past research on chloride diffusion in concrete generally focused on specimens with artificial cracks and did not express the real condition and real shape of concrete cracks. Digital image processing technology provides an innovative method for considering the microstructure influences on transport properties in rock and geotechnical materials. Image analysis technology was used to represent rock structures (Zhang et al.) in COMSOL. It has also been employed to couple with a finite element method for the two-dimensional mechanical analysis of geomaterials (Yue et al. 2003). However, there is no systematic procedure available to simulate the cracked concrete corrosion process using a 3-D digital image-based microstructure model.

In this study, approaches for obtaining an understanding of diffusion and binding (reaction) in cracked concrete using the COMSOL Multiphysics package are presented. Two different 3-D microstructures with cracks were employed in the simulations. A 3-D X-ray CT image-based mortar microstructure was measured and a 3-D virtual microstructure using a spherical harmonic analysis-based approach (Garboczi 2002) was created. The 3-D image-based microstructure and spherical harmonic-based microstructure both were converted into a finite element mesh form using recent techniques developed for random microstructures (Lu and Garboczi). Next, a 3-D mesh representing the true multiphase microstructure was written as a Nastran mesh and imported into the COMSOL Multiphysics package. Two COMSOL interfaces, Transport of Diluted Species and User Defined ODE Mathematics, were employed in this study to examine the influence of cracking on chloride diffusion with binding. For the purpose of validation, a micro X-ray fluorescence ( $\mu$ XRF) (Janssens et al. 1996) test was performed to measure the chloride concentration profile of a mortar sample at NIST and compare the experimental to simulation results. Then, the 3-D X-ray CT image-based microstructure and the 3-D virtual microstructure were both used to study the crack effect on chloride transport.

## 2. Image-based Microstructures

Two different representations of microstructures with cracks were employed to compute transport and absorption binding (reaction). The microstructure study focused on concrete composed of a matrix of cement paste (hydrated cement), sand and gravel inclusions (aggregates), and voids. The two microstructures considered here are (a) X-ray computed tomography (CT) images of a mortar stacked into a 3-D digital image, and (b) real-shaped sand and gravel particles, represented by spherical harmonic series, randomly placed into a 3-D box to make a virtual concrete microstructure. Based on recent 3-D meshing procedures (Lu and Garboczi), the microstructures with a crack could be generated.

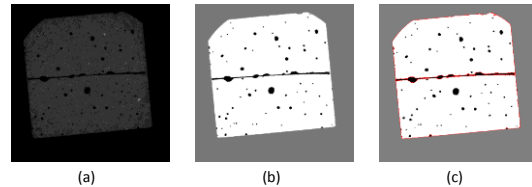


**Figure 1.** Two-dimensional slices (25 mm x 25 mm mortar sample with water-to-cement ratio of 0.4) from 3-D microtomographic image data set corresponding to: (a) - original X-ray CT image slice, (b) - segmented multiphase image, and (c) - crack region is segmented from other phases and the crack area is shown with a red outline. The voxel size is 0.017 mm.

The first microstructure is a 3-D microstructural representation based on 2-D images taken at NIST, as obtained using X-ray computed microtomography (CT). For each sample scanned, a three-dimensional computational volume is divided into a cubic grid of voxels, where each voxel contains a single phase (mortar, crack and voids). Figure 1 provides two-dimensional slices of the X-ray CT data set. The specimen contains three readily distinguishable phases based on different grey level intensity values (or more correctly x-ray absorption): dark air voids and empty pores, dark crack, and bright mortar (cement paste). The sizes and shapes of many of the individual air voids are readily observed, both in their two-dimensional (Figures 1) and in their three-dimensional (Figure 2) forms. Most of these empty pores were air voids entrained during sample preparation. The largest connected dark

area is the crack phase. The crack was made by putting a stainless steel shim into the casting specimen from the top, and then pulling it out after final set of the mortar has occurred. One should note that individual aggregates could not be distinguished from the matrix in these images. Optimizing the X-ray CT instrument in order to be able to see and segment the aggregates is an area of future work.

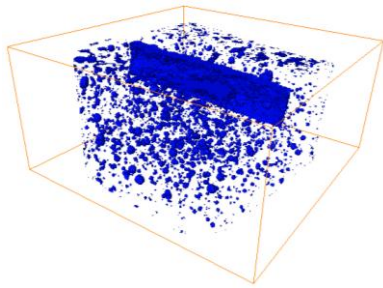


**Figure 2.** Three-dimensional volume rendering of crack and voids from segmented images. The 3-D volume rendering image indicates regions where the top crack and voids distribution are present in the specimen.

To perform a detailed quantitative analysis, the image set was processed and analyzed as follows. First, to reduce the random noise present in the three-dimensional image set, each image was processed using a median filter. In applying a median filter, each voxel (image element) within the specimen volume is replaced by the median (grey level) value for all voxels within a fixed size cube centered on the voxel being considered. Median filters remove noise by smoothing the data, while preserving small details and sharp edges. After filtering operations, the grey level histogram (a plot of the number of voxels containing each grey level intensity value vs. grey level intensity) was determined for this image data set. Next, the image data set was segmented into 3 phases, voids, crack, and cement paste. Finally, the 3-D surface mesh and 3-D volumetric mesh were created from the segmented three-phase images.

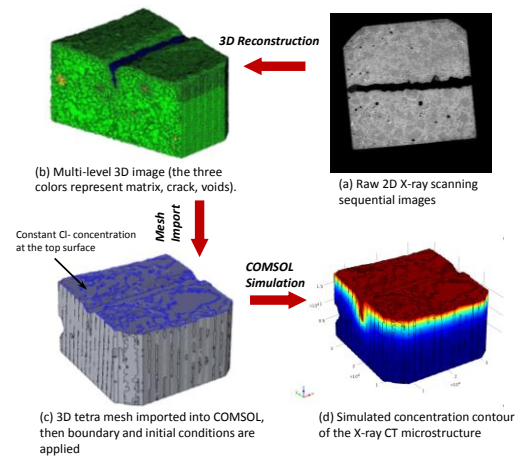


**Figure 3.** Three-dimensional diffusion and binding simulation procedure with an X-ray microtomography image set; cubic specimens were 25 mm on a side.

Figure 3(a-c) shows a schematic of 3-D reconstruction, mesh import and COMSOL simulation for the X-ray CT image-based microstructure. Figure 3(d) plots the simulation result of the X-ray CT image-based microstructure, the last step in the simulation procedure. This cracked concrete sample was entirely covered by an (impermeable) epoxy layer except at the top surface. As shown in Figure 3, the original image data set was 2000 x 2000 x 985 voxels, with each voxel representing 17  $\mu\text{m}$ . The intensity histogram measured on each phase in the two-dimensional images is utilized to reconstruct a representative three-dimensional microstructure with the same voids ratio, surface area, volume, and correlation as the original concrete. This original data set was used to create a 3-D finite element mesh (Lu and Garboczi). The final 3-D tetrahedral mesh contained a total of 120689 nodes and 615166 tetrahedral elements, including 573691 mortar elements, 34695 crack elements, and 6780 void elements.

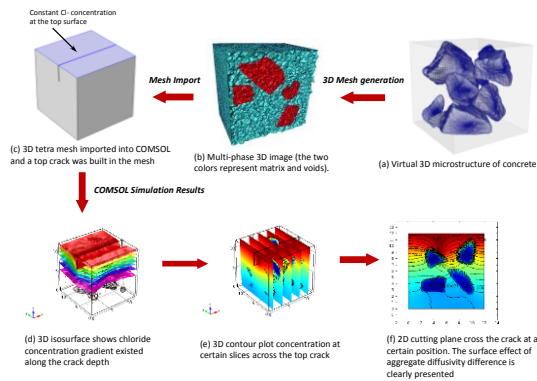


**Figure 4.** Three-dimensional virtual concrete simulation made by real aggregates represented in spherical harmonic analysis. The virtual concrete model has 12 irregular shape aggregates from the VCCTL database (Bentz et al. 2006; Bullard and Garboczi 2006; Bullard and Stutzman 2006; Zhihui et al. 2007), and a built-in crack, which is located on the top surface of the sample.

The second microstructure is a virtual concrete model, which was built using a random particle placement program (Qian 2012), as shown in Figure 4. This is a simulation volume containing only two phases, a mortar matrix and irregular shape aggregates. This microstructure was developed to study mechanical and transport properties, e.g. represent interaction between concrete aggregates and their surrounding interfacial transition zones, as well as extended to numerous other concrete applications. The microstructure represents a three-dimensional cube of concrete or mortar grains, depending on the size chosen. In this application, the aggregate size distribution was chosen to match that of coarse aggregates in real concrete materials. A model representing a 12 mm x 12 mm x 12 mm cube of concrete was created, requiring 12 individual particles randomly placed in this specimen to represent a realistic coarse aggregate size distribution and obtain a coarse aggregate volume fraction of 18.2 %. The matrix is assumed to be mortar. To study the influence of cracks, one can build various shaped cracks into the virtual concrete model. In constructing the cracked model, a rectangular crack (100 μm x 3 mm x 12 mm) was built in the specimen at the top surface. The schematic of the 3-D virtual concrete microstructure is also shown in Figure 4 (a-c), illustrating the 3-D mesh generation, mesh import and COMSOL simulation steps. Figure

4(d-f) schematically plots the isosurface, sliced concentration, and 2-D cutting plane of the virtual concrete microstructure simulation results.

### 3. Transport and Binding Model

#### 3.1 The basic chloride diffusion equation

Usually chloride ions diffuse into concrete from the external environment. The physical model considered in this study includes diffusion and sorption binding (reaction) processes, which is a non-steady state process. Provided that concrete is a semi-infinite homogeneous medium in a saturated state, the chloride ingress process is often described by Fick's second law. The one-dimensional diffusion equation can be expressed as (Martín-Pérez et al. 2000; Yuan et al. 2009):

$$\frac{\partial C_t}{\partial t} = \frac{\partial}{\partial x} \left( D \frac{\partial C_f}{\partial x} \right) \quad (1)$$

where  $C_t$  is the total chloride concentration and  $t$  is time,  $D$  is the effective diffusion coefficient and  $C_f$  is the free chloride concentration at depth  $x$ .

For the case of one-dimensional diffusion with no binding/reaction and a constant diffusion coefficient  $D$ , the following analytical solution for diffusion, according to Fick's second law in a semi-infinite media, can be utilized to estimate the concentration of chloride ions as a function of depth and time (Crank 1979):

$$\frac{C(x,t)}{C_s} = 1 - \operatorname{erf} \left( \frac{x}{\sqrt{2Dt}} \right) \quad (2)$$

where  $C(x,t)$  is the chloride content at the depth  $x$  at a given time  $t$ ,  $\operatorname{erf}()$  represents the error function,  $C_s$  is the chloride concentration at the top surface of the concrete, and  $D$  is the chloride ion diffusion coefficient in the concrete. In this form, the utility of plotting results as dimensionless variables, namely  $C(x,t)/C_s$  vs.  $x/(\sqrt{2Dt})$ , is apparent. Equation (2) provides a convenient analytical solution to evaluate the validity of one-dimensional finite element or finite difference models for diffusive transport. Additionally, if the chloride

concentration necessary to initiate corrosion at a known depth of reinforcement  $x$  is supplied, along with the concrete diffusion coefficient and the surface chloride concentration, Equation (2) can be solved to determine the estimated service life, defined to be the time  $t$  to achieve this concentration at depth  $x$ .

### 3.2 Chloride binding capacity

Chloride binding is significant to the chloride transport process, and can be an important factor in predicting the service life of concrete structures. The binding effect does not modify the steady-state chloride diffusion coefficient. Chloride binding just leads to an increase in the time lag (Truc et al. 2000) and thus potentially in the service life. The total chloride content includes free chloride and bound chloride. According to the conservation of mass equation, the relationship between total chloride and free chloride can be described by:

$$C_{total} = C_{bound} + C_{free} \quad (3)$$

where  $C_{free}$  is the free chloride concentration,  $C_{bound}$  is the bound chloride concentration, and  $C_{total}$  is the total chloride concentration.

While Freundlich, Langmuir, and linear isotherms (Luping and Nilsson 1993) have all been employed in past studies of chloride binding in concrete, for these simulations, a simple linear isotherm was utilized to express the relationship between free and bound chlorides:

$$C_{bound} = \alpha C_{free} \quad (4)$$

where  $\alpha$  is a fitting parameter, here taken to be equal to 4, as obtained by fitting the experimental data (30 d and 90 d exposures) for a mortar specimen with no cracks (Bentz et al. 2012; Sahmaran and Yaman 2008). This is the best fit value for Equation (4) when  $C_{free}$  and  $C_{bound}$  are both expressed in units of  $\text{mol Cl}^- / \text{m}^3$  pore solution. The single isotherm equation was utilized to model the combined effects of sorption of the chloride ions by the calcium silicate hydrate gel (C-S-H) and other hydration products, as well as the reaction of these ions with aluminate phases present in the hydrated cement paste. This sorption/reaction is implemented in COMSOL Multiphysics by

adding a reaction term to the standard diffusion equation, resulting in:

$$\frac{\partial C}{\partial t} = \nabla \cdot (D \nabla C) + k(C_{bound} - \alpha C_{free}) \quad (5)$$

The simulation in COMSOL Multiphysics was performed using Equation (5), as implemented in the Transport of Diluted Species and User Defined ODE Mathematics interfaces; the diffusion and rate constants are provided in Table 1.

### 3.3 Boundary and initial conditions

Both irregular and regular cracks can influence chloride ingress, since both can be included in a general microstructure. Both the crack width and depth are important parameters that may control the diffusion in the numerical simulation. A wider crack provides a higher concentration of chloride ions, while a deeper crack provides a longer easy-diffusion channel for the chloride ions, both of which affect the chloride concentration gradients within the concrete's interior. In reinforced concrete, a deep crack leads to an easier path for chloride ions to approach the rebar surface, causing depassivation and ultimately corrosion. The schematic of applying a constant chloride concentration at the top surface of the two 3-D cracked microstructures are shown in Figure 3(c) and Figure 4(c), respectively. Employing a constant concentration chloride source fixed at the sample top surface, we simulated a ponding test of chloride ingress. For chloride transport in both of the models, the top surface of the specimen was kept at a constant chloride concentration of  $1170 \text{ mol/m}^3$ . The other surfaces were assumed to be impermeable, experimentally by using an epoxy layer coating, designed to block chloride diffusion during the measurement. Therefore, we specified a zero flux boundary condition at the bottom surface and at side surfaces. Since binding (reaction) only takes place within the mortar/concrete part, no reactions take place within the crack area. The initial concentration in the crack was set to  $1170 \text{ mol/m}^3$ , the constant ponding value, because the concentration in the crack will be quickly made equal to the ponding value via convection. The concrete microstructure can have a strong influence on the chloride concentration distribution. To study the diffusion effects of each particular phase, a different chloride

diffusivity was assigned to different phases in each of the microstructures. There are bulk mortar, voids, and crack phases in the X-ray CT microstructure, while the spherical harmonic-based microstructure contains bulk mortar, non-porous (no diffusion) aggregates, and crack phases. The initial bound chloride contents in both crack and matrix are zero, since the chloride ions do not bind until they penetrate into the concrete. It is assumed that the aggregate is free of binding (reaction) effects, so, the binding effect only takes place in the mortar region.

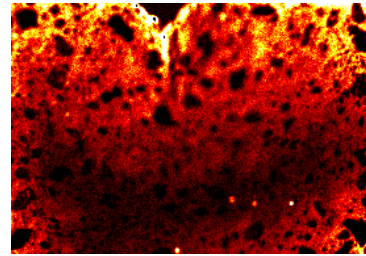
**Table 1.** Parameters used in COMSOL simulations

Parameter	Calibrated value
Diffusion coefficient of bulk mortar	$6 \times 10^{-11} \text{ m}^2/\text{s}$
Sorption rate constant in bulk mortar	$3 \times 10^{-7} \text{ s}^{-1}$
Diffusion coefficient in crack	$2 \times 10^{-9} \text{ m}^2/\text{s}$
Diffusion coefficient in voids	$0.001 \text{ m}^2/\text{s}$
Diffusion coefficient in non-diffusive aggregates	$0.001 \text{ m}^2/\text{s}$
$\alpha$ parameter in linear isotherm	4
External chloride concentration	$1170 \text{ mol/m}^3$
Assumed porosity of mortar	0.1828

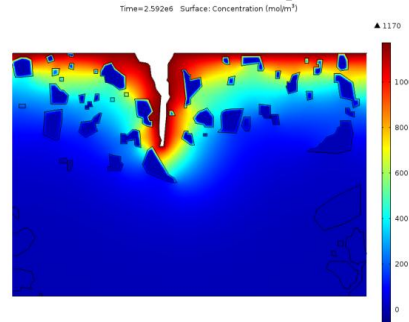
The parameters used in the COMSOL Multiphysics simulations, as obtained by calibration against an existing experimental data set for cracked mortars (Sahmaran and Yaman 2008), are summarized in Table 1. The calibration results are presented in (Bentz et al. 2012). To analyze chloride ion diffusion and the resulting concentration profile, the COMSOL Multiphysics package implements the UMFPAK direct solver. Therefore, COMSOL analyzed the diffusion equation discussed in the model section, and coupled this with the binding (reaction) equation for the dependence of binding rate on concentration. The time step used was 0.01 s for a total simulation time of 30 d.

## 4 Results

### 4.1 Micro-XRF technique measurement validation



(a) Micro-XRF measurement plot for chloride



(b) 2-D chloride ingress contour

**Figure 5.** Micro-XRF measurement result of chloride concentration contour plot and the 2-D chloride ingress simulation contour comparison

Valuable information for model validation was obtained by comparison with  $\mu$ XRF measurement data of the following experiment. We prepared an experimental test with a chloride ponding on the mortar specimen surface. For the purpose of blocking the chloride from the bottom and side surfaces, an epoxy layer was coated on all surfaces of the sample, except the top surface. Then, the surface was exposed to a salt solution at a constant concentration for 30 d, driving the chloride ions into the sample. The  $\mu$ XRF technique rapidly measures the elemental composition of a sample by irradiating it with a thin beam of X-rays without disturbing the sample. Using  $\mu$ XRF, we could detect the chlorine concentration on the concrete sample as a function of spatial location with a resolution of about 20  $\mu\text{m}$ .

The chloride concentration within an exposed mortar cube was measured following a previously established protocol (Bentz et al. 2009). When the chloride ponding test finished, the cubic sample was broken into half and the  $\mu$ XRF technique used to measure the chloride concentration profile of the broken surface, without requiring any polishing or other specimen preparation. In Figure 5, the origin is

taken at the top left corner, with the x-axis running horizontally increasing to the right and the z-axis vertically, with z increasing in the downward direction. The surfaces were 25 mm wide and 17 mm high. The relevant chloride concentration was determined from chloride ion profile measurements obtained on the specimen, as shown in Figure 5(a). Micro-XRF measurements were obtained along the z direction at certain values of x. The top surface crack shown as a black triangle is located at the upper part of the specimen. It is seen that black areas, representing pores, voids, or low diffusivity aggregates, of different sizes are located throughout the  $\mu$ XRF chloride image, because the chloride ions diffuse much less in those parts than in the cement paste. The white/light yellow represents the higher concentrations, while the dark red depicts lower concentrations. The profile changes gradually from the top to the bottom surface. To obtain the 2-D mesh, the 2-D image data analysis technology was used on the  $\mu$ XRF image to create an appropriate triangular mesh. Employing the diffusion and reaction parameters shown in Table 1, COMSOL simulation results depicted in Figure 5(b) shows good agreement with the  $\mu$ XRF measurement. This implies a reasonably good solution of the diffusion and binding physical model and a validation of the parameters in Table 1.

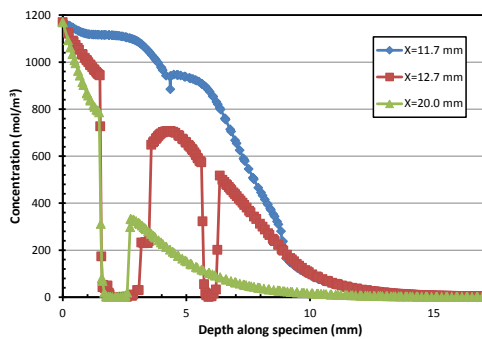


**Figure 6.** The concentration value at cutting line along  $X=11.7$ ,  $12.7$ , and  $20.0$  mm of 30 days

To compare the crack effect on the chloride concentration gradient distribution, vertical lines located at three different values of x were made to plot the simulation results. Figure 6 gives the plotted simulation results of these concentration profiles. The highest curve shows the data at

$X=11.7$  mm, which is right along the crack surface. While away from the crack surface, the other two curves at  $X=12.7$  mm and  $X=20$  mm show that the concentration curve gradually drops down as distance increases, which shows that the crack serves as an accelerated path for chloride ion diffusion. It is noted that two abrupt steps appear in the middle curve ( $X=12.7$  mm), representing the numerical path traversing across the non-diffusive aggregates in the sample. The abrupt steps shown in the other two curves ( $X=11.7$  mm and  $X=20$  mm) also show this non-diffusive aggregate effect. It is also noteworthy that the chloride concentration in the  $\mu$ XRF measurement image is not exactly consistent with the modeling contour, especially at the areas along both side surfaces and the bottom surface. That was because the epoxy surface coating employed in this first study was found to not completely block the chloride ingress in the real specimens. So, some chloride ion diffusion from the sides and bottom can be seen in Figure 5(a).

#### 4.2 X-ray CT microstructure

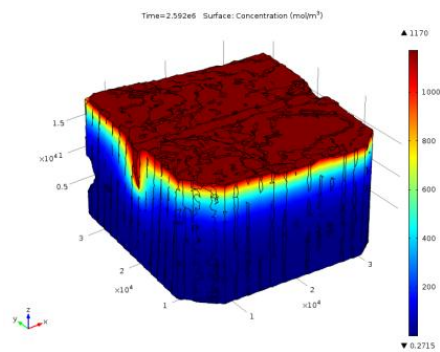


**Figure 7.** Concentration contour plot of 3-D X-Ray image-based model at 30 day

For the 3-D X-ray CT microstructure simulation, bulk mortar, voids, and crack phases were considered. Using the validated diffusion and reaction parameters listed in Table 1, the concentration contour plot at 30 d is shown in Figure 7. Since the constant concentration boundary condition was applied on the top surface, there is a higher concentration in the upper part, while exhibiting a lower value at the bottom. The crack effect can also be seen from the contour plot. This is a roughly V-shape

irregular crack. It has a sharp crack tip, but the crack mouth is an open entrance for chloride ions at the surface. Since the chloride ingress into intact mortar is a slow process, the chloride concentration profile, shown in Figure 7, at the vicinity of crack tip has a sharp front and changes smoothly which is in accord with the experimental observations, as illustrated in Figure 5(a).

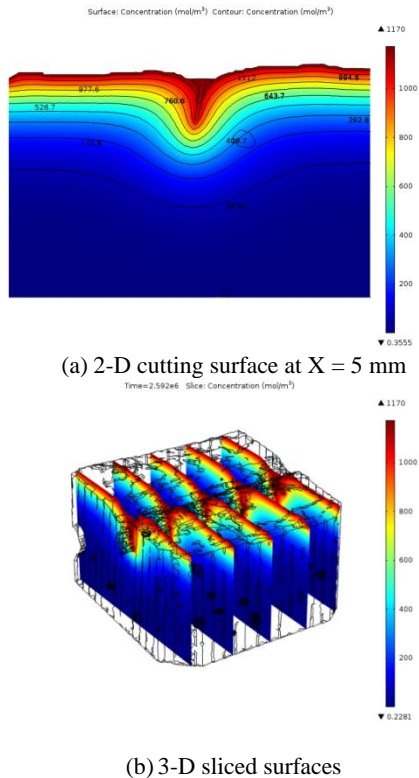


**Figure 8.** Concentration contour plot of 3-D X-Ray image-based concrete model simulation result at 30 day

Figure 8 illustrates the concentration contour plot for the X-ray CT-based simulation results, where (a) shows the 2-D slice cutting surface at X=5 mm and (b) depicts sliced surfaces transverse to the crack length. From Figure 8, we can see that crack has an obvious effect on the concentration profile serving as an ingress channel for chloride ions. These figures provide a qualitative means to model validation.

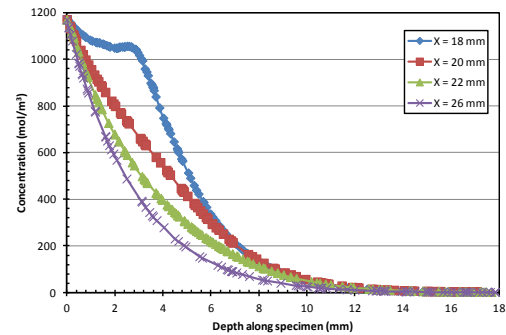


**Figure 9.** Concentration profile along the crack depth, the straight cutline arranged from the closest to the farthest away from the crack area, (Y=20 mm, X=18 mm, 20 mm, 22 mm, 26 mm, Z= cross depth)

To compare the crack effect on the concentration gradient distribution, data was sampled at four fixed values in the X direction (X=18 mm, 20 mm, 22 mm, and 26 mm). Figure 9 shows the plotted simulation results of concentration profiles along the sample depth at these four locations as a function of z or the depth of penetration. The highest curve was taken at X =18 mm, which is close to the crack surface. It is observed that a peak appears at three mm depth, which shows a sharp diffusivity difference between the crack and the mortar phase. While away from the crack surface (see the other three curves at X= 20 mm, 22 mm, and 26 mm), the concentration curves gradually decrease as the depth increases, typical of a Fickian diffusion behavior. Although a non-diffusive void phase was considered in this simulation, it did not much affect the chloride concentration profile due to the small size and limited number of voids in the X-ray microstructure. Since we do not account for the non-diffusive aggregate phase, the mortar is considered a uniform phase and individual aggregate is not recognized in this case.

### 4.3 Virtual concrete microstructure

To further explore the diffusivity difference between aggregate and cement paste, the virtual concrete microstructure was also simulated in the COMSOL Multiphysics package. As listed in Table 1, a smaller diffusivity value was given to the aggregate, while a much larger value was used in the mortar matrix. The simulation was run with a constant concentration boundary

condition at the top surface, the same as in the X-ray CT microstructure. After a simulated 30 d period, the chloride ingress into the virtual concrete sample is shown in Figure 10. It can be seen from the sliced contour (a) and the iso-surfaces (b) that aggregates with low diffusivity result in low concentration values. The diffusion gradient can also be seen from the top to bottom, which is similar to the X-ray CT microstructure simulation. The chloride concentration contour was highly influenced by the built-in crack, leading to a V-shape profile along the crack depth.

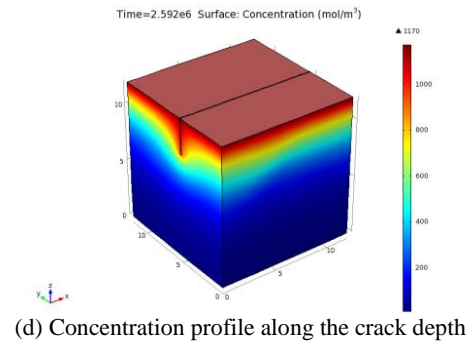
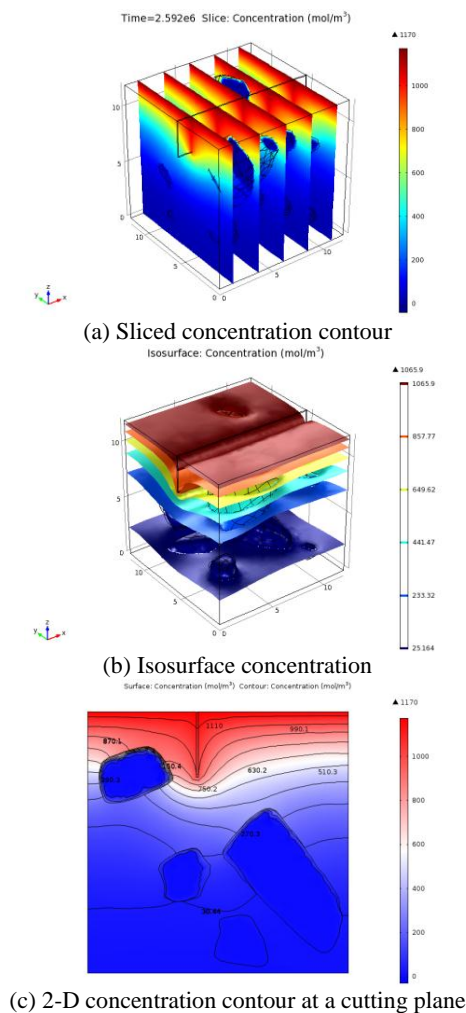


**Figure 10.** Concentration contours of 3-D virtual concrete model simulation result, shown in sliced contour, isosurface and 2-D cutting surface, and overall profile

In addition to the 3-D overall concentration profile shown in Figure 10 (d), we also made a 2-D cutting slice across the crack at a certain position ( $X = 5$  mm), illustrated in Figure 10(c). The chloride concentration changes sharply at the aggregate surface, as the low diffusivity aggregate is clearly presented. The dense iso-surface curve at the aggregate surface shows a very sharp concentration change. In regard to the crack effect, it is also observed that the built-in crack leads to a quick ingress channel of saturated chloride solution. The profile slope changes sharply along the crack depth, while returning to a flat shape with increasing the distance from the crack. To study the acceleration effect caused by the built-in crack, a sound concrete sample (no crack) was also simulated by COMSOL. Figure 11 shows the comparison between the sound and the cracked virtual concrete models. The results are displayed at three different locations at fixed  $X$  ( $X=5$  mm, 6 mm, 8 mm) on the cracked sample and at  $X = 5$  mm on the uncracked sample. Comparing the non-crack and cracked curves, it is observed from Figure 11 that a crack in the concrete has a severe accelerating effect on the chloride diffusion. A sharp diffusivity difference between the crack and mortar phase is also observed. While away from the crack surface (see the other three curves at  $X=5$  mm, 6 mm, and 8 mm), the concentration curves gradually decrease as the depth increases. The presence of aggregates, as indicated by a sharp drop in the concentration values to zero, are clearly in the

two X=5 mm (at 6.5 mm depth) and the X=8 mm (at 4.5 mm depth) curves.

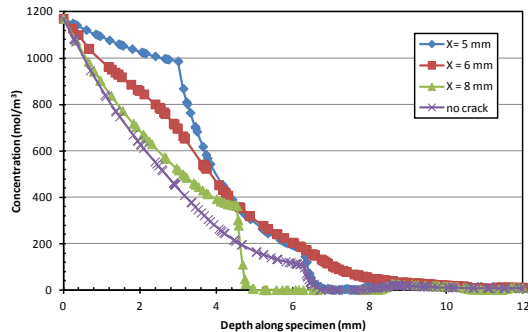


**Figure 11.** Concentration profile plot at cutting line long (Y=5 mm, X=5 mm, 6 mm, and 8 mm, Z = cross depth), comparing non-cracked specimen at cutting line long (Y=5 mm, X=5 mm, Z = cross depth)

## Conclusions

We presented one  $\mu$ XRF measurement and three examples of chloride ingress simulations. Both X-ray CT image-based and spherical harmonic based microstructures were successfully applied to build heterogeneous cracked concrete models. Chloride ingress processes in these cracked heterogeneous concrete microstructures were accurately simulated with the COMSOL Multiphysics package. It was observed that cracks in concrete can have an accelerating effect on the chloride diffusion, while the sorption binding (reaction) generally retards the chloride penetration (Bentz et al. 2012). In other words, the cracks would act as an accelerator (conductor), while binding would act as a moderator. Hence, the behavior of chloride transport in cracked concrete media depends strongly on whether there is a crack and on the inherent binding capability of the concrete.

Confidence in the simulations was gained by comparing to the  $\mu$ XRF measurements. Experiments carried out to validate numerical models must have clear boundary and initial conditions, geometry and well-defined material properties. As concerns the image-based  $\mu$ XRF measurements, all such requirements are met. The real microstructure of the 2-D  $\mu$ XRF image was accounted for in the simulation and the simulation result shows good agreement with the  $\mu$ XRF measurement. Hence, the chloride

transport mathematical descriptions and image-based cracked concrete microstructures were validated in terms of their ability to reproduce the natural chloride ingress processes.

We have thus demonstrated that using the COMSOL package for the simulation of transport and binding of chloride ions in cracked concrete produces interesting results, validated by  $\mu$ XRF experiments, and thus is useful for the analysis of chemical ingress in fractured concrete.

## References

- Bentz, D., Garboczi, E., Lu, Y., Martys, N., Sakulich, A., and Weiss, J. (2012). "Modeling of the Influence of Transverse Cracking on Chloride Penetration into Concrete (submitted to Cement and Concrete Composites)."
- Bentz, D. P., Garboczi, E. J., Bullard, J. W., Ferraris, C. F., and Martys, N. S. "Virtual testing of cement and concrete." *Proc., Significance of Tests and Properties of Concrete and Concrete-Making Materials*, ASTM STP 169D
- Bentz, D. P., Peltz, M. A., Snyder, K. A., and Davis, J. M. (2009). "VERDiCT: Viscosity Enhancers Reducing Diffusion in Concrete Technology." *Concrete International*, 31(1), 31-36.
- Bullard, J. W., and Garboczi, E. J. (2006). "A model investigation of the influence of particle shape on portland cement hydration." *Cement and Concrete Research*, 36(6), 1007-1015.
- Bullard, J. W., and Stutzman, P. E. (2006). "Analysis of CCRL proficiency cements 151 and 152 using the virtual cement and concrete testing laboratory." *Cement and Concrete Research*, 36(8), 1548-1555.
- Crank, J. (1979). *The mathematics of diffusion*, Oxford University Press, Oxford, [Eng].
- Garboczi, E. J. (2002). "Three-dimensional mathematical analysis of particle shape using X-ray tomography and spherical harmonics: Application to aggregates used in concrete." *Cement and Concrete Research*, 32(10), 1621-1638.
- Janssens, K., Vekemans, B., Vincze, L., Adams, F., and Rindby, A. (1996). "A micro-XRF spectrometer based on a rotating anode generator and capillary optics." *Spectrochimica Acta Part B-Atomic Spectroscopy*, 51(13), 1661-1678.
- Kwon, S. J., Na, U. J., Park, S. S., and Jung, S. H. (2009). "Service life prediction of concrete wharves with early-aged crack: Probabilistic approach for chloride diffusion." *Structural Safety*, 31(1), 75-83.
- Lu, Y., and Garboczi, E. "Bridging the gap between VCCTL based CAD and CAE using STL files."

- ASCE Journal of Computing in Civil Engineering* (under review).
- Luping, T., and Nilsson, L.-O. (1993). "Chloride binding capacity and binding isotherms of OPC pastes and mortars." *Cement and Concrete Research*, 23(2), 247-253.
- Marsavina, L., Audenaert, K., Schutter, G., Faur, N., and Marsavina, D. (2009). "Experimental and numerical determination of the chloride penetration in cracked concrete." *Construction and Building Materials*, 23(1), 264-274.
- Martin-Pérez, B., Zibara, H., Hooton, R. D., and Thomas, M. D. A. (2000). "A study of the effect of chloride binding on service life predictions." *Cement and Concrete Research*, 30(8), 1215-1223.
- Pan, T., and Lu, Y. (2012). "Stochastic Modeling of Reinforced Concrete Cracking due to Nonuniform Corrosion: FEM-Based Cross-Scale Analysis." *JOURNAL OF MATERIALS IN CIVIL ENGINEERING*, 24(6), 698-706.
- Perko, J., Seetharam, S., and Mallants, D. "Verification and validation of flow and transport in cracked saturated porous media." *Proc., The Proceedings of 2011 COMSOL Conference in Stuttgart*.
- Qian, Z. (2012). "Multiscale Modeling of Fracture Processes in Cementitious Materials." PhD thesis, Delft University of Technology.
- Richter, M., Moenickes, S., Richter, O., and Schröder, T. "The Soil as a Bioreactor: Reaction-Diffusion Processes and Biofilms." *Proc., The Proceedings of 2011 COMSOL Conference in Stuttgart*.
- Sahmaran, M., and Yaman, I. O. (2008). "Influence of transverse crack width on reinforcement corrosion initiation and propagation in mortar beams." *Canadian Journal of Civil Engineering*, 35(3), 236-245.
- Truc, O., Ollivier, J. P., and Carcassès, M. (2000). "A new way for determining the chloride diffusion coefficient in concrete from steady state migration test." *Cement and Concrete Research*, 30(2), 217-226.
- Yuan, Q., Shi, C., De Schutter, G., Audenaert, K., and Deng, D. (2009). "Chloride binding of cement-based materials subjected to external chloride environment – A review." *Construction and Building Materials*, 23(1), 1-13.
- Yue, Z. Q., Chen, S., and Tham, L. G. (2003). "Finite element modeling of geomaterials using digital image processing." *Computers and Geotechnics*, 30(5), 375-397.
- Zhang, S., Saxena, N., and Barthelemy, P. "Poromechanics Investigation at Pore-scale Using Digital Rock Physics Laboratory." *Proc., The Proceedings of 2011 COMSOL Conference in Stuttgart*.
- Zhihui, S., Garboczi, E. J., and Shah, S. P. (2007). "Modeling the elastic properties of concrete composites: Experiment, differential effective medium theory, and numerical simulation." *Cement and Concrete Composites*, 29(1).